

Dalton Transactions

Accepted Manuscript



This is an *Accepted Manuscript*, which has been through the Royal Society of Chemistry peer review process and has been accepted for publication.

Accepted Manuscripts are published online shortly after acceptance, before technical editing, formatting and proof reading. Using this free service, authors can make their results available to the community, in citable form, before we publish the edited article. We will replace this *Accepted Manuscript* with the edited and formatted *Advance Article* as soon as it is available.

You can find more information about *Accepted Manuscripts* in the [Information for Authors](#).

Please note that technical editing may introduce minor changes to the text and/or graphics, which may alter content. The journal's standard [Terms & Conditions](#) and the [Ethical guidelines](#) still apply. In no event shall the Royal Society of Chemistry be held responsible for any errors or omissions in this *Accepted Manuscript* or any consequences arising from the use of any information it contains.

Structural and magnetic properties of the ruthenium double perovskites $\text{Ba}_{2-x}\text{Sr}_x\text{YRuO}_6$

Ben Ranjbar, Adriano Parvan and Brendan J. Kennedy,*

School of Chemistry, The University of Sydney, Sydney, NSW 2006, Australia

Zhaoming Zhang

Australian Nuclear Science and Technology Organisation, Lucas Heights, NSW 2234, Australia

Abstract

The crystal structures of the series of ordered double perovskites $\text{Ba}_{2-x}\text{Sr}_x\text{YRuO}_6$ ($0 \leq x \leq 2$) were studied by high resolution synchrotron X-ray diffraction. The materials displayed a sequence of structures $Fm\bar{3}m$ ($a^0a^0a^0$) $\xrightarrow{x=0.6}$ $I4/m$ ($a^0a^0c^-$) $\xrightarrow{x=1.0}$ $I2/m$ ($a^-a^-c^0$) $\xrightarrow{x=1.4}$ $P2_1/n$ ($a^-a^-a^+$) associated with increasing tilting of the corner sharing octahedra. The same sequence of structures can be induced by varying the temperature of appropriate members of the series. Magnetic susceptibility measurements demonstrate the oxides to be antiferromagnets with a Neel temperature of $\sim 30\text{K}$. There is a simple correlation between the Weiss constant θ and the Ru-O-Y bond angle. The two Sr rich oxides ($x = 1.8$ and 2.0) display an, unusual, sharp minimum in susceptibility at low temperatures that is associated with the reorientation of the spins.

Introduction

Much of the contemporary interest in the mixed metal $A_2BB'O_6$ double perovskites, where A is an alkaline earth cation (Ca, Sr or Ba) and B/B' a transition metal or lanthanoid, stems from their fascinating physical properties that include superconductivity¹, tunnelling magnetoresistance^{2,3} and high temperature ferrimagnetism⁴. Magnetic B -type cations in the $A_2BB'O_6$ structure can form a face-centered-cubic (FCC) lattice that, if the exchange between the nearest cations is AFM, satisfies the criteria for geometric frustration⁵⁻⁷. Geometrically frustrated magnetic materials can possess exotic ground states including spin-liquids, spin-glasses and spin-ice and there is evidence for such in Ru containing double perovskites^{8,9}.

The structures of Sr_2YRuO_6 and Ba_2YRuO_6 were first described around 30 years ago, whereas Sr_2YRuO_6 has a monoclinic structure in space group $P2_1/n$, Ba_2YRuO_6 is cubic in

$Fm\bar{3}m$ ^{10, 11}. In both cases there is a 1:1 rock-salt like ordering of the pentavalent Ru⁵⁺ cations, which have a high spin 4d³ electron configuration, and the diamagnetic Y³⁺ cations. The rock-salt type ordering of the smaller *B* and *B'*-type cations in the $A_2BB'O_6$ double perovskite structure alters the symmetry from $Pm\bar{3}m$, in the ABO_3 perovskite aristotype, to $Fm\bar{3}m$ ^{12, 13}. The monoclinic symmetry in Sr₂YRuO₆ is a result of cooperative rotations of the corner sharing octahedra which arise due to the non-optimal relative sizes of the *A*- and *B*-type cations, as quantified by the perovskite tolerance factor $t = (r_A + r_O) / \sqrt{2}(r_{B^*} + r_O)$, where r_{B^*} is the averaged ionic radii of the *B* and *B'* cations. The tilt pattern in Sr₂YRuO₆ is the same as that observed in SrRuO₃¹⁴.

The crystal and magnetic structures of Sr₂YRuO₆ were established by Battle and Mackin¹¹, using neutron diffraction, who reported the magnetic moment of the Ru⁵⁺ cations to be $\mu = 1.85\mu_B$. This is noticeably less than the spin only value of 3.87 μ_B . Bulk susceptibility measurements, obtained well above the Neel Temperature, give an experimental moment of 3.15 μ_B whilst at low temperatures much smaller values were deduced, possibly due to spin disorder associated with magnetic frustration. Singh and Tomy described a remarkable reversal in the magnetisation of polycrystalline samples at low magnetic fields^{15, 16}. The negative values of magnetisation observed at the lowest temperatures are reminiscent of a superconductor although bulk conductivity measurements show Sr₂YRuO₆ as non metallic. Doping Sr₂YRuO₆ has been reported to result in superconductivity^{17, 18}.

A second unusual feature of Sr₂YRuO₆ is the presence of two low temperature transitions in heat capacity measurements near 28 and 24 K.¹⁹ Bernardo and co-workers¹⁹ suggested that these are structural in origin and drive magnetic transitions of the Ru⁵⁺ cations as a consequence of a delicate balance between ferromagnetic (FM) and anti-ferromagnetic (AFM) interactions that lead to a local reversal of the spin and loss of spin collinearity. Neutron diffraction studies, however, show evidence for a single transition²⁰.

Heat capacity measurements reveal a single low temperature transition in Ba₂YRuO₆ at 37 K.²¹ This corresponds to the onset of the AFM ordering observed in the neutron diffraction experiments with the Ru moment being similar to that seen for Sr₂YRuO₆, $\mu = 2\mu_B$ at low temperatures^{5, 10}. Aharen and co-workers²¹ presented bulk susceptibility measurements that suggest a second transition near 47 K and found evidence for short range magnetic correlations above T_N.

Evidently chemical pressure, introduced by the use of a smaller *A*-site cation, alters the structure and details of the magnetic properties of the Ru double perovskites, but this does not appear to have been systematically studied. The aim of the present work is to establish the evolution in the structure and magnetic properties in the series $\text{Ba}_{2-x}\text{Sr}_x\text{YRuO}_6$. In particular we seek to establish the importance of geometric factors in a series with a constant magnetic cation.

Experimental

Polycrystalline samples of $\text{Ba}_{2-x}\text{Sr}_x\text{YRuO}_6$ were prepared by solid state reaction. The appropriate stoichiometric mixtures of BaCO_3 (Aldrich, 99.999%), SrCO_3 (Aldrich, 99.99%), Y_2O_3 (Aithaca, 99.999%) and Ru metal (Aithaca, 99.9%) were weighed and finely mixed by hand in an agate mortar. The powders were placed in alumina crucibles and heated as follows: 12 hrs at 650 °C and 12 hrs at 850 °C with intermediate regrinding. After mixing again the powders were pressed into 20 mm pellets and heated in air at 1050 °C for 24 hours, 1200 °C for 72 hrs and finally at 1400 °C for 72 hrs. The samples were cooled to room temperature in the furnace over a period of several hours.

Synchrotron X-ray powder diffraction (S-XRD) data were collected over the angular range $5^\circ < 2\theta < 85^\circ$, using X-rays of wavelength 0.8260 Å, on the powder diffractometer at BL-10 beamline of the Australian Synchrotron²². The samples were housed in 0.2 mm diameter capillaries that were rotated during the measurements. Temperature control was achieved using a Cyberstar hot-air blower (RT- 1300 K) or Oxford Cryosystems Cryostream Plus (90-400 K). Once the control sensor had reached the set point temperature, data collection was commenced after a 3 min thermal equilibration period; thermal stability was of the order ± 2.0 K for all data collection temperatures. The data were obtained using a bank of 16 Mythen detectors, each of which covers around 5 degrees of data. Diffraction data were collected for five minutes at two detector positions to avoid gaps in the data from the individual modules. Rietveld-refinements against the S-XRD data were carried out using the GSAS program with the EXPGUI front-end²³. Scale factors, zero-shifts, background functions, and single Lorentzian broadening terms on top of the standard pseudo-Voigt peak shape functions for the instruments were refined in addition to the unit cell parameters.

X-ray absorption near edge structure (XANES) spectra at the Ru and Y L-edges were collected on the Soft X-ray Beamline at the Australian Synchrotron²⁴. Powder samples were thinly dusted onto double-sided carbon tape (SPI Supplies) and inserted into the vacuum

chamber *via* a load lock. The pressure inside the analysis chamber was maintained at better than $\sim 10^{-9}$ torr. Spectra were collected in both fluorescence yield (FY) and total electron yield (TEY) mode, although the FY is very weak at the Ru L₃-edge (as its energy is near the end of the designed range of the beamline). For energy calibration purpose, all spectra were taken simultaneously with a TEY signal measured from a reference material, either Ru(OH)Cl₃ or Y₂O₃, positioned upstream in the beamline. This reference removed approximately 10% of the beam intensity away from the sample. The energy calibration at the Ru L₃-edge was based on setting the peak height of the Ru(OH)Cl₃ reference XANES spectra at 2840.1 eV (Ru(OH)Cl₃ was itself calibrated against Ru metal with the maximum of the first derivative set to 2838 eV),²⁵ whereas the Y L₃-edge spectra were calibrated by setting the maximum of the first derivative of the Y L₂-edge spectrum of the Y₂O₃ reference at 2155 eV (which corresponds to 2079.4 eV at the Y L₃-edge)²⁶. All XANES spectra were analysed using the Athena software program.²⁷

DC magnetic susceptibility data were measured using a Quantum Design Physical Properties Measurement System (PPMS). Data were collected from 300 to 4 K in a field of 1000 Oe using the vibrating sample magnetometer (VSM) technique. The same device was used for the heat capacity measurements using a thermal relaxation method.

Results and Discussion

i. Room Temperature Structures

Establishing the correct symmetry of perovskites can be challenging using X-ray diffraction. Cooperative tilting of the octahedra involves small displacements of the anions, quantification of which can be difficult where heavy atoms such as Ru ($Z = 44$) or Ba ($Z = 56$) are present. A further complication is the tendency of numerous perovskites to exhibit high pseudo symmetry, which can be beyond the modest detection capability of many diffractometers. High resolution synchrotron X-ray diffraction (S-XRD) can negate these problems. The narrow peak widths of the S-XRD patterns provide sensitivity to small changes in the cell metric whilst the exceptional signal-to-noise afforded by the X-ray diffractometer employed in this work enabled the identification of weak reflections associated with lowering of the symmetry through octahedral tilting. In this work S-XRD was employed to initially identify the most appropriate space group. Having established the cell metric and space group, the structures were obtained by Rietveld refinement.

Portions of the synchrotron X-ray powder diffraction profiles for 11 samples in the series of $\text{Ba}_{2-x}\text{Sr}_x\text{YRuO}_6$, recorded at room temperature, are shown in Figure 1. This figure shows a systematic shift in the position of the peaks to higher angles as the Sr content is increased, as expected given the smaller size of Sr^{2+} compared with Ba^{2+} (ionic radii 1.44 vs 1.61 Å for 12-coordinate). The *R*-point reflection near $2\theta = 19.5^\circ$ (indexed as 311 in $Fm\bar{3}m$), evident in Figure 1a, gains its intensity from a combination of *B*-site cation ordering and out-of-phase octahedral tilting. The extreme weakness of this in the S-XRD pattern of Ba_2YRuO_6 reflects the absence of such tilts and the small difference in the electron numbers between $\text{Y}^{3+} 4d^0$ and $\text{Ru}^{5+} 4d^3$. The presence of such *R*-point reflections is indicative of doubling of the perovskite unit cell with the appropriate space group being $Fm\bar{3}m$. As the Sr content is increased to 0.6, the (440) reflection near $2\theta = 33^\circ$ is observed to develop a shoulder ultimately resolving into a doublet whilst the (222) reflection near $2\theta = 20^\circ$ remains a singlet and no additional reflections appear. The splitting of the (222) and related reflections demonstrates a lowering of symmetry and that this is a doublet suggests the structure is tetragonal. Through examination of the early work of Howard the appropriate space group is $I4/m$.¹³ The (222) reflection would not split if the symmetry was rhombohedral. Increasing the Ba content beyond $x = 0.8$ results in splitting of the (222) reflection into a triplet which requires the symmetry to be monoclinic. Critically at $x = 1.0$ only *R*-point reflections are evident in the diffraction pattern, showing that only out-of-phase tilting of the corner sharing octahedra is present and from Howard's group theory analysis the appropriate space group is identified as $I2/m$. Further increasing the Sr content to $x = 1.4$ results in the appearance of additional superlattice reflections that are identified as *M*- and *X*-point reflections. The *M*-point reflections are a consequence of in-phase octahedral tilting whilst the *X*-point reflections require both in-phase and out-of-phase tilts to be present. It is concluded that the Sr rich oxides are monoclinic in $P2_1/n$.

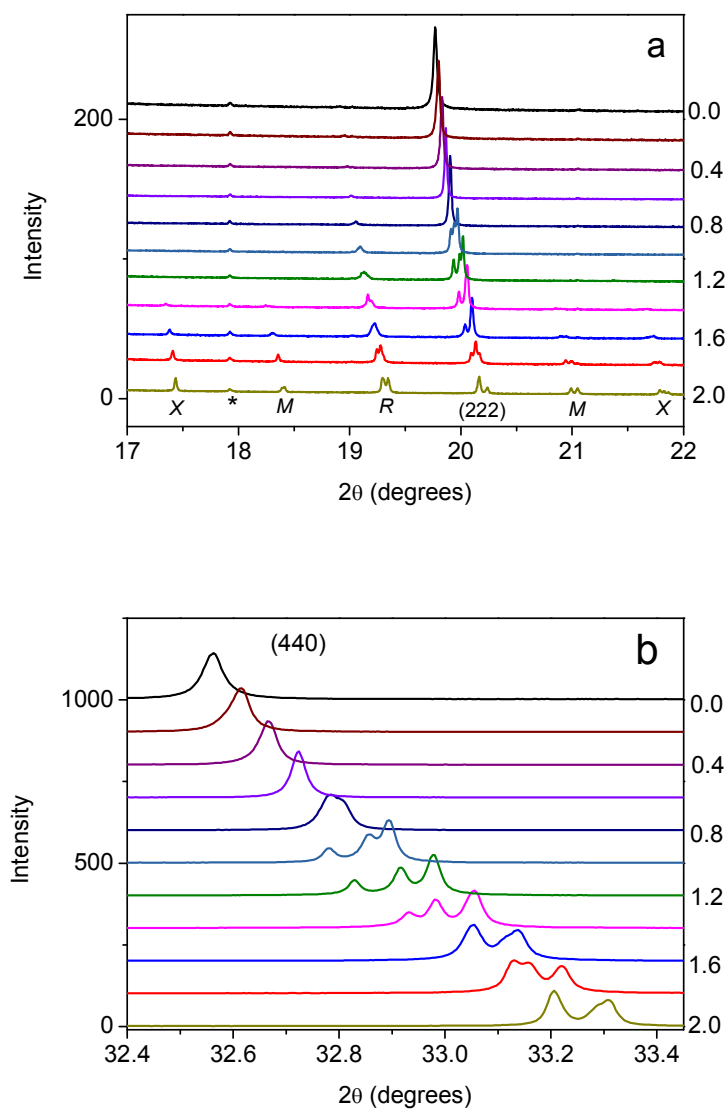


Figure 1. Composition dependence of portions of the S-XRD patterns for $\text{Ba}_{2-x}\text{Sr}_x\text{YRuO}_6$ from $x = 0$ (top) to $x = 2$ (bottom). The development of superlattice reflections associated with cooperative tilting of the corner sharing octahedra is illustrated in (a) while the splitting of the (440) reflection indicative of the cell metric is illustrated in (b). For the origin of the labels X , R and M , see the text. The peak labelled * is due to a trace amount of Y_2O_3 in the sample.

The sequence of phases observed in $\text{Ba}_{2-x}\text{Sr}_x\text{YRuO}_6$ is thus:

$Fm\bar{3}m (a^0 a^0 a^0) \xrightarrow{x=0.6} I4/m (a^0 a^0 c^-) \xrightarrow{x=1.0} I2/m (a^- a^- c^0) \xrightarrow{x=1.4} P2_1/n (a^- a^- a^+)$. This sequence was verified by Rietveld refinements and these results are summarised in Table 1 and the four structures are illustrated in Figure 2.

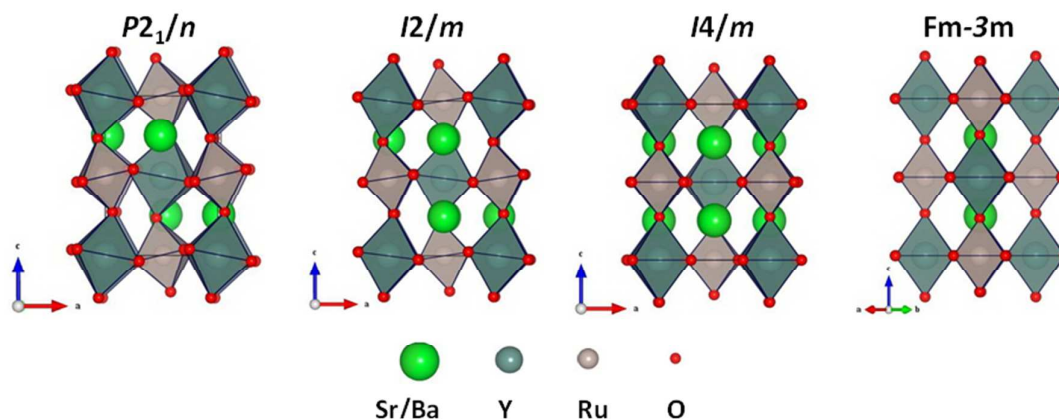


Figure 2. Representations of the structures of the four structural modifications observed in the series $Ba_{2-x}Sr_xYRuO_6$.

Typical examples of the Rietveld refinements are illustrated in Figure 3. This sequence of phases is also found upon cooling the samples to 90 K with the phase boundary shifted and is the same as that observed in a number of other double perovskite families including A_2NiWO_6 ²⁸, A_2CoWO_6 ²⁹ and A_2InTaO_6 ³⁰. Of the three observed transitions, the $I4/m$ to $I2/m$ transition, which involves a reorientation of the out-of-phase tilts from [001] to [110], must be first order¹³. Conversely the $Fm\bar{3}m \rightarrow I4/m$ and $I2/m \rightarrow P2_1/n$ transitions, involve the introduction of a new tilt and are allowed to be continuous¹³. Narayanan and co-workers³¹ reported the same sequence of structures in the series $La_{2-x}Sr_xCoIrO_6$, but described the $I2/m \rightarrow P2_1/n$ transition as being first order. Transitions between two perovskite structures that differ only in their pattern of octahedral tilts that are allowed to be continuous are observed, almost invariably, to be continuous. This suggests that the changes in the oxidation state play a significant role in driving the $I2/m \rightarrow P2_1/n$ transition in $La_{2-x}Sr_xCoIrO_6$ series. That valence state changes can drive first order phase transitions in perovskites is evident from studies of Ba_2TbRuO_6 ³² and $Ba_3BiRu_2O_9$ ^{25,33}. In the present case the ruthenium must remain pentavalent as yttrium can only be 3+.

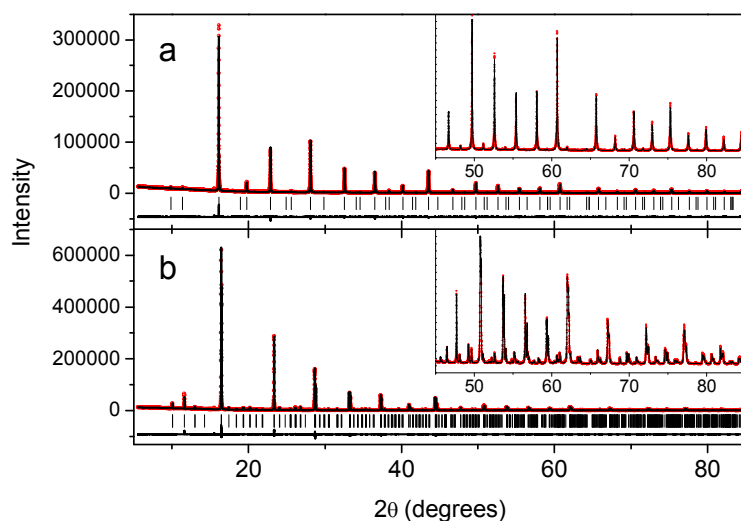


Figure 3. Representative Rietveld refinement profiles for (a) Ba₂YRuO₆ and (b) Sr₂YRuO₆. The symbols are the experimental data and the solid line the fit to the profile. In each case the difference between the observed and calculated profiles is given as the lower solid line, and the vertical markers show the positions of the space group allowed Bragg reflections. The insets highlight the quality of the data and fits to high angles.

ii. Variable Temperature Structural Studies

The temperature dependence of the Sr₂YRuO₆ structure is summarised in Figure 3. The structure of Sr₂YRuO₆ remains monoclinic upon heating to 1300 K, however as illustrated in Figure 4, whilst the thermal expansion of the cell volume is unexceptional the expansion of the individual lattice parameters is anisotropic such that the three reduced lattice parameters become approximately equal near 900 K before diverging again above this. Judging by the temperature dependence of the monoclinic angle a continuous transition to a higher symmetry structure appears remote, fitting this to an expression of the type $\beta - 90 = A(T_c - T)^{0.5}$ ³⁴ suggests the transition temperature T_c is around 2300 K, well above the decomposition temperature of the material.

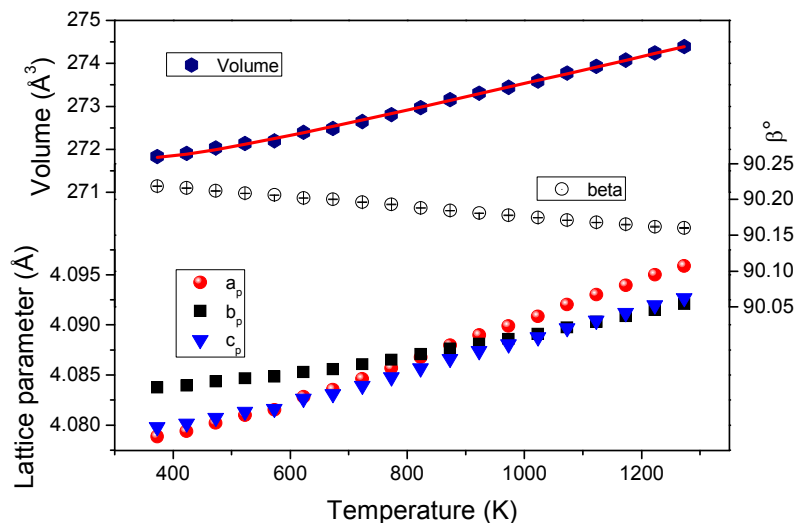


Figure 4. Temperature dependence of the unit cell volume, monoclinic angle and appropriately scaled lattice parameters for Sr_2YRuO_6 . Where not apparent the errors are smaller than the symbols.

Conversely the temperature dependence of the $x = 0.8$ sample $\text{Ba}_{1.2}\text{Sr}_{0.8}\text{YRuO}_6$ shows two phase transitions, namely $Fm\bar{3}m \xrightarrow{450\text{ K}} I4/m \xrightarrow{200\text{ K}} I2/m$ as shown in Figure 5. The latter transition is characterised by an extensive two-phase ($I4/m + I2/m$) region indicative of a first order phase transition. $\text{Ba}_{1.4}\text{Sr}_{0.6}\text{YRuO}_6$ is cubic at 300 K and transforms to the tetragonal $I4/m$ structure just below this, retaining this structure as the sample is cooled to 90 K. Conversely $\text{Ba}_{1.0}\text{Sr}_{1.0}\text{YRuO}_6$ is monoclinic in $I2/m$ at 300 K, transforming to tetragonal $I4/m$ near 400 K and ultimately cubic near 550 K. Evidently chemical pressure mimics the effect of lowering the temperature in terms of the observed phase transitions.

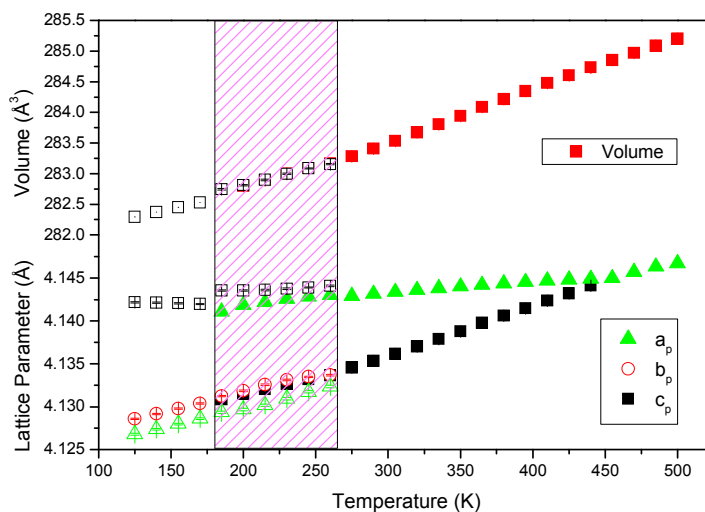


Figure 5. Temperature dependence of the unit cell volume and scaled lattice parameters for $\text{Ba}_{1.2}\text{Sr}_{0.8}\text{YRuO}_6$. The shaded area indicates the region where the tetragonal $I4/m$ (solid symbols) and monoclinic $I2/m$ (open symbols) phases co-exist. Where not apparent the errors are smaller than the symbols.

iii. XANES Spectra

Bond valence calculations indicate that both the Y and Ru are overbonded (i.e. BVS greater than the nominal oxidation state) with the Ru showing greater discrepancy, see Table 1. The BVS for the A-type cations are unexceptional, e.g. 2.00 at $x = 0.0$ and 1.85 at $x = 2.0$. The oxidation states of the Y and Ru cations were probed using the L_3 -edge XANES spectroscopy. The Y and Ru L_3 -edge XANES spectra of the series $\text{Ba}_{2-x}\text{Sr}_x\text{YRuO}_6$ are shown in Figures 6 and 7 respectively, resulting from dipole-allowed transitions from the cation $2p_{3/2}$ orbitals to the unoccupied $4d$ states. Because the Y($4d$) and Ru($4d$) states are directly involved in Y-O and Ru-O bonding, information on their oxidation states and local symmetry can be obtained from the absorption edge energy and the shape of the L_3 -edge XANES spectra respectively.^{25, 26, 35, 36} As shown in Figures 6 and 7, each L_3 -edge spectrum displays a bimodal feature (corresponding to t_{2g} - and e_g -related states of the octahedrally coordinated B-site cations), and there are no changes in the absorption energy at either the Y or Ru L_3 -edge across the series. Both the absorption energy and appearance of the Y and Ru L_3 -edge spectra confirm that only trivalent Y and pentavalent Ru are present in the current samples.^{37,}

³⁸ In addition Figure 6 shows that, although the t_{2g} position at the Y L_3 -edge does not change,

the e_g peak does shift slightly towards lower energy with increasing Sr content in the samples. This is consistent with increased local disorder around Y atoms with the substitution of Sr for Ba, as the crystal structure evolves from cubic to tetragonal then to monoclinic. Similar observations were made recently at the Zr L_3 -edge for $Y_2(\text{Sn,Zr})_2\text{O}_7$ that the crystal field splitting of the Zr($4d$) orbitals decreases when the local environment around Zr deviates more from an octahedral site.³⁵ Interestingly, the reduced local symmetry around Ru atoms does not result in observable peak shift at the Ru L_3 -edge (Figure 7). This may be attributed to the fact that the crystal field splitting of the Ru($4d$) orbitals is not as large as that of the Y($4d$) orbitals (*i.e.*, the energy difference between the t_{2g} and e_g peaks is smaller), therefore subtle changes in the peak position might be more difficult to detect.

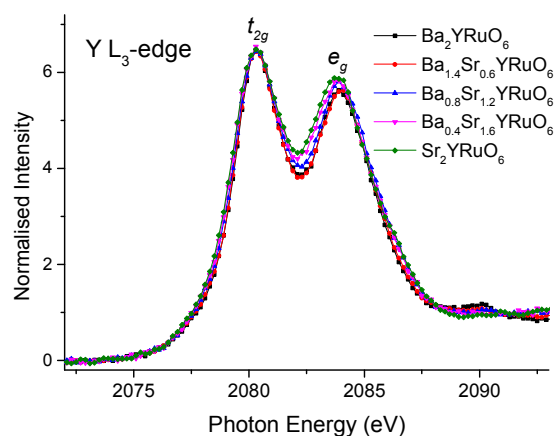


Figure 6. Normalised Y L_3 -edge XANES spectra collected in FY mode from representative samples in the $\text{Ba}_{2-x}\text{Sr}_x\text{YRuO}_6$ series: $x = 0$ (cubic structure in $Fm\bar{3}m$), $x = 0.6$ (tetragonal structure in $I4/m$), $x = 1.2$ (monoclinic structure in $I2/m$), $x = 1.6$ and 2.0 (monoclinic structure in $P2_1/n$).

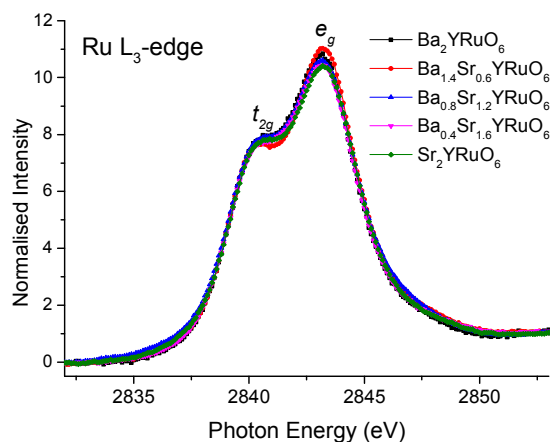


Figure 7. Normalised Ru L₃-edge XANES spectra collected in TEY mode from representative samples in the Ba_{2-x}Sr_xYRuO₆ series: $x = 0$ (cubic structure in $Fm\bar{3}m$), $x = 0.6$ (tetragonal structure in $I4/m$), $x = 1.2$ (monoclinic structure in $I2/m$), $x = 1.6$ and 2.0 (monoclinic structure in $P2_1/n$).

iv. Magnetic Susceptibilities

The temperature dependence of the field cooled (FC) and zero-field cooled (ZFC) magnetic susceptibilities for Ba_{2-x}Sr_xYRuO₆ is illustrated in Figure 8. In the FC magnetic susceptibility (upper figure) we observe that, as described previously¹⁰, Ba₂YRuO₆ shows AFM ordering with $T_N = 37$ K. We find that, at low Sr contents ($x < 1.2$) T_N decreases as Sr is added to the sample, see arrow in the upper right figure). As the Sr content is increased further the susceptibility shows a rapid increase more reminiscent of ferromagnetism (upper left figure), although the ground state is antiferromagnetic. The temperature dependence of the ZFC susceptibilities (lower figure) is more striking. Again at low Sr contents the behaviour is typical of AFM, and whilst not obvious from Figure 8, there is little branching of the FC and ZFC susceptibilities. The ZFC susceptibilities for Sr₂YRuO₆ are remarkably different, and show a narrow peak near 30 K and a well defined minimum near 25 K. As described by Garcia and Ghivelder⁹ the temperatures of the two peaks in the heat capacity of Sr₂YRuO₆ are in good agreement with the maximum and minimum observed in the ZFC susceptibilities, Similar behaviour is observed for Ba_{0.2}Sr_{1.8}YRuO₆ although the magnitude of the minimum is noticeably less.

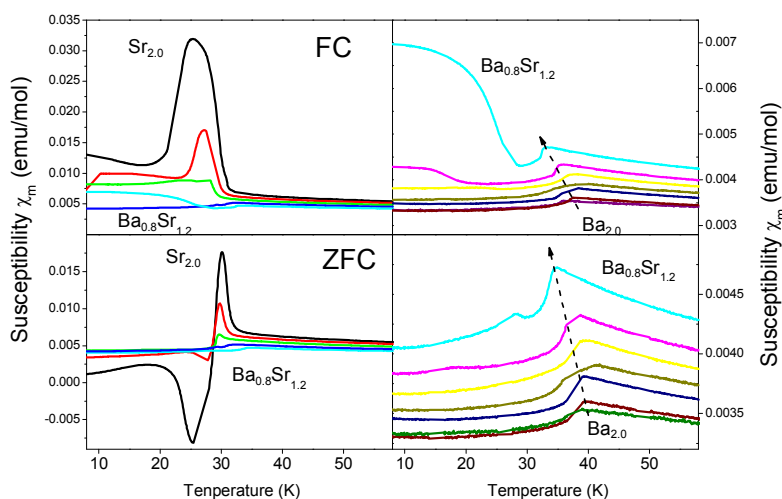


Figure 8. Temperature dependence of the FC (upper) and ZFC (lower) magnetic susceptibilities for $\text{Ba}_{2-x}\text{Sr}_x\text{YRuO}_6$, in all panels the Sr content decreases in 0.2 steps from top to bottom. Note the different y-scales, with the data for $\text{Ba}_{0.8}\text{Sr}_{1.2}\text{YRuO}_6$ duplicated in the panels. The arrow in the right-hand panels highlights the gradual trend of decreasing T_N with increasing Sr content.

Discussion

The structures of the two end-members Sr_2YRuO_6 and Ba_2YRuO_6 refined here from S-XRD data are in remarkably good agreement with those described in earlier neutron diffraction studies^{10,11}. The precision of the refinements is remarkable given the presence of the heavy Ru and Y cations. That this degree of accuracy and precision is achieved in the present work reflects both the signal-to-noise ratios of the diffraction data, which affords well resolved superlattice reflections (see Figure 1a) that are sensitive to the anion displacements, and the high resolution $d_{\min} = 0.61 \text{ \AA}$ ($2\theta=85^\circ$ at $\lambda=0.825 \text{ \AA}$). Such resolution is impossible with Cu K_α radiation ($\lambda = 1.54 \text{ \AA}$; $d_{\min} = 0.77 \text{ \AA}$ at $2\theta=180^\circ$).

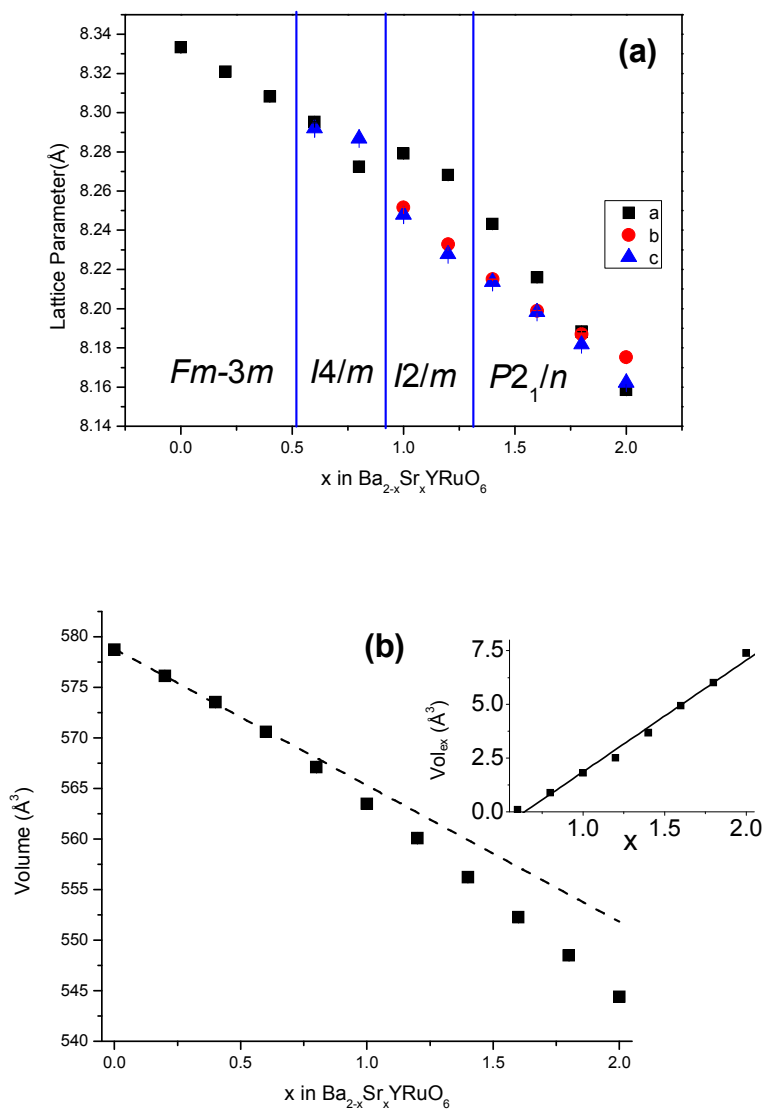
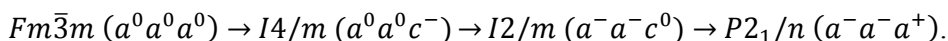


Figure 9. (a) Composition dependence of the scaled unit cell parameters and (b) volume of Ba_{2-x}Sr_xYRuO₆. The dotted line is the best fit to the volume of the three cubic samples. In inset is the excess volume, calculated by subtracting the observed volume from the value estimated from the linear fit.

The observed sequence of structures is consistent with the group theory analysis¹³ where the symmetry is initially altered from $Pm\bar{3}m$ to $Fm\bar{3}m$ by the ordering of the Ru and Y cations. As the average size of the *A*-type cation is reduced, out-of-phase tilting about [001] initially occurs lowering the symmetry to tetragonal. At a critical composition the direction

of the out-of-phase tilts switches from [001] to [110], resulting in a decrease in symmetry to monoclinic. Ultimately in-phase tilts are introduced and the observed sequence is



The reorientation of the out-of-phase tilts that characterises the first order $I4/m - I2/m$ transition results in a reversal of the c/a ratio (Figure 9a). Despite the first order tetragonal to monoclinic transition occurring near $x = 1.0$, as is evident from Figure 9, there is no apparent discontinuity in the volume as the composition is altered (Figure 9b). Rather, a progressive deviation from Vegard's Law (linear dependence of volume on size, *i.e.*, Sr content) is evident in Figure 9b with the volume of the lower symmetry structures being less than that estimated from a linear extrapolation of the volumes for the cubic oxides. This decrease in the volume is a consequence of strain associated with the tilting of the BO_6 octahedra, and as shown from the inset in Figure 9b there is a linear relationship between the excess volume, calculated simply by subtracting the observed volume from that estimated by a linear extrapolation from the cubic structures, and composition suggesting the $Fm\bar{3}m \rightarrow I4/m$ transition is continuous³⁹.

The continuous nature of the $I2/m - P2_1/n$ transition is evident from the changes in the monoclinic angle β . Illustrated in Figure 10 is the composition dependence of the monoclinic angle and this is seen to vary as $\beta - 90^\circ \propto (x - x_0)^{0.5}$ ³⁹ where x is the Sr content and x_0 the composition at which the transition to tetragonal occurs (at $x \sim 0.8$).

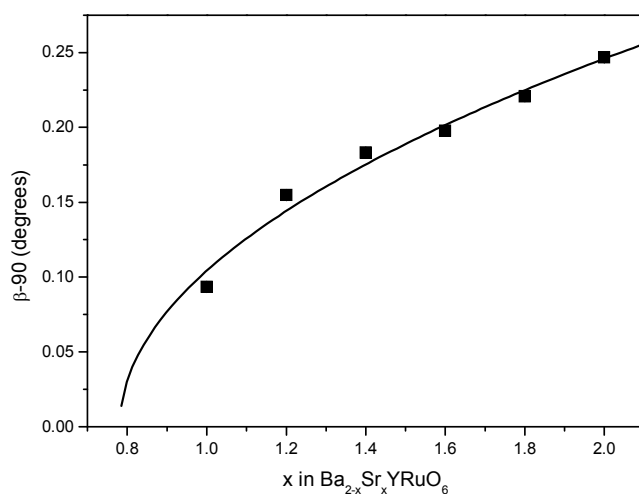


Figure 10 Composition dependence of the monoclinic angle as ($\beta-90$) in the series $\text{Ba}_{2-x}\text{Sr}_x\text{YRuO}_6$. The solid line is the best fit to an expression of the type $\beta - 90^\circ \propto (x - x_0)^{0.5}$ where x is Sr content and x_0 is the critical composition indicative of a second order transition.

Whilst the present S-XRD data are not sufficient to provide accurate estimates of the tilts, the lattice parameters are extremely precisely determined. It is well established that the strains introduced by the tilting of the octahedra can be quantified by the distortion of the cell metric where the linear strain components e_1 , e_2 and e_3 for the $I4/m$ structure are given by:⁴⁰

$$e_1 = e_2 = \frac{a_{pc} - a_o}{a_o} = \frac{\left(\frac{a}{\sqrt{2}} - a_o\right)}{a_o}, \quad e_3 = \frac{c_{pc} - a_o}{a_o} = \frac{\left(\frac{c}{2} - a_o\right)}{a_o}$$

Here $a_o (=V_o^{1/3})$ is the lattice parameter of the cubic structure extrapolated to lower temperatures. The symmetry-adapted tetragonal strains, e_t , is a combination of the linear strain components, e_1 , e_2 , e_3 :

$$e_t = \frac{1}{\sqrt{3}}(2e_3 - e_1 - e_2) = \frac{c - \sqrt{2}a}{\sqrt{3}a_o},$$

As evident from Figure 11 the plot of this against temperature is linear for $\text{Ba}_{1.2}\text{Sr}_{0.8}\text{YRuO}_6$ showing the transition to be second order³⁹. The tetragonal strain for $\text{Ba}_{1.0}\text{Sr}_{1.0}\text{YRuO}_6$ also showed a linear dependence with temperature, with a higher critical temperature of 573 K.

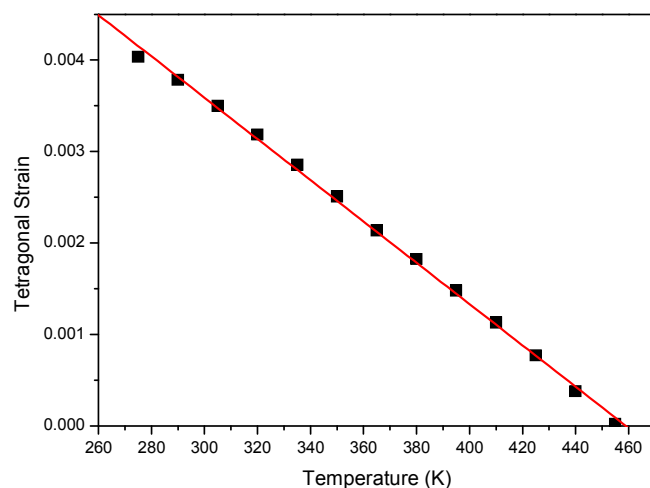


Figure 11. Temperature dependence of the symmetry-adapted tetragonal strain, e_t , for $\text{Ba}_{1.2}\text{Sr}_{0.8}\text{YRuO}_6$. The solid line is a linear fit.

The magnetic susceptibilities of the 11 samples were investigated under both field cooled (FC) and zero-field cooled (ZFC) conditions (Figure 8). The data in the paramagnetic region were analysed using a linear Curie-Weiss fit from which the Weiss constant was determined. The fits were also used to calculate the effective moment per formula unit and these values are included in Table 1. The observed magnetic moments ranged from 4.2 to 3.7 μ_B which are in good agreement with the spin-only value for the d^3 Ru^V ion (3.87 μ_B). The moments are greater in the Ba rich oxides and it is postulated that this is due to local compositional inhomogeneities (anti-site disorder) leading to weak ferromagnetic interactions. Given the negligible difference in the X-ray scattering factors of Y³⁺ and Ru⁵⁺ it is not possible to detect such disorder using single wavelength XRD data, although disorder has been observed in the related Ca₂LnRuO₆ series^{41,42}. The Weiss constants are strongly dependent on the composition ranging from -540 K at $x = 0.0$ to -270 K at $x = 2.0$.

There have been numerous attempts to correlate structures with magnetic properties and, despite most structures being determined at temperatures well above the magnetic transition temperature, phenomenological models have been developed. In the present case, the approximately tetragonal oxygen coordination of the Ru cations totally removes the degeneracy of the e_g levels and partially lifts that of the t_{2g} levels. This distortion favours the $t_{2g}(\pi)$ - $e_g(\sigma)$ mixing that broadens the widths of the 4d(Ru/Y)-2p(O) sub-bands, W . The band width can be estimated from the empirical relationship $W \approx \cos \omega / 3.5l$, where l is the average of the different B -O and B' -O bond lengths and ω the average (Y,Ru) - O - (Y,Ru) bond angle. This formula was originally proposed to correlate structural and magnetic properties in manganites,⁴³ but has subsequently been successfully used to quantify changes in the A₂FeMoO₆ double perovskites⁴⁴.

There is a complex compositional dependence of the average B -O distance, shown in Fig. 12. The average B -O distance initially decreases as the smaller Sr cation is introduced to the structure, reaching a minimum near $x = 0.8$, that is close to where the composition induced $Fm\bar{3}m$ to $I4/m$ transition occurs. This is accompanied by an increase in the BVS of the Ru with that of the Y remaining approximately constant (Table 1). Tilting of the octahedra initially increases the average B -O distance (and concurrent decrease in the BVS), providing a more stable bonding environment for the ions. Initially the tilting simply counteracts the impact of the reduced cell volume on the average bond distances, but ultimately the average B -O distance is observed to increase, presumably to reduce the extent

of overbonding of the cations, as was also seen in the series $\text{Ba}_{1-x}\text{Sr}_x\text{SnO}_3$.⁴⁵ The composition dependence of W mirrors that of the average bond distance, initially it increases as the Sr content increases until about $x = 0.8$ above which it decreases, however the derived Weiss constants do not show a simple relationship with W rather we observe a simple linear relationship between that and the Ru-O2-Y bond angle, Figure 13. This angle can be taken as a proxy for the octahedral tilting distortion. The in-plane Ru-O2-Y tilting angle in Ba_2YRuO_6 is 180° and this reduces to 157.9° in Sr_2YRuO_6 (Table 1), noting that in the cubic structure all the oxygen atoms are crystallographically equivalent whereas in the monoclinic structure there are three distinct types of oxygen atoms. The structural distortion is expected to weaken the superexchange magnetic interaction between Ru ions via the Ru-O-Y-O-Ru or Ru-O-O-Ru pathway and consequently lower the Weiss constants. This expectation is clearly met, as Figure 13 shows the Weiss constant θ decreasing as the Ru-O2-Y angle increases. This correlation, whilst pleasing, is possibly enhanced since the value of θ was estimated from the high temperature Curie-Weiss fit.

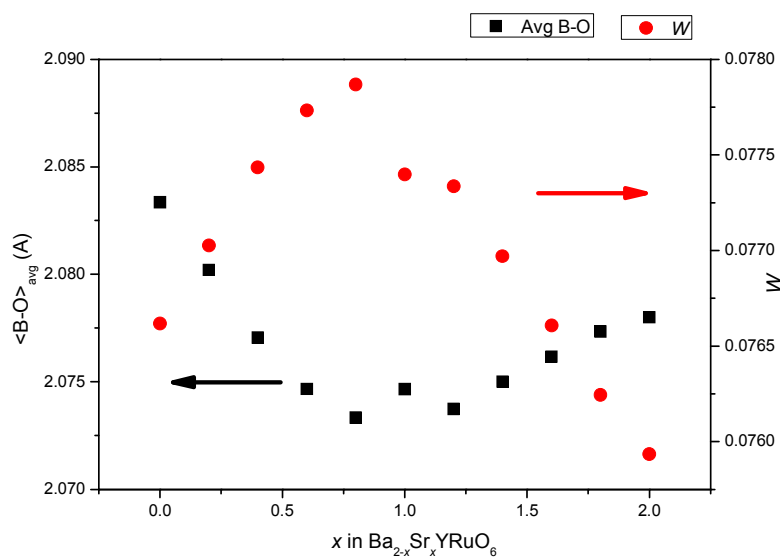


Figure 12. Composition dependence of the average B -O bond distance and band width W in the series $\text{Ba}_{2-x}\text{Sr}_x\text{YRuO}_6$.

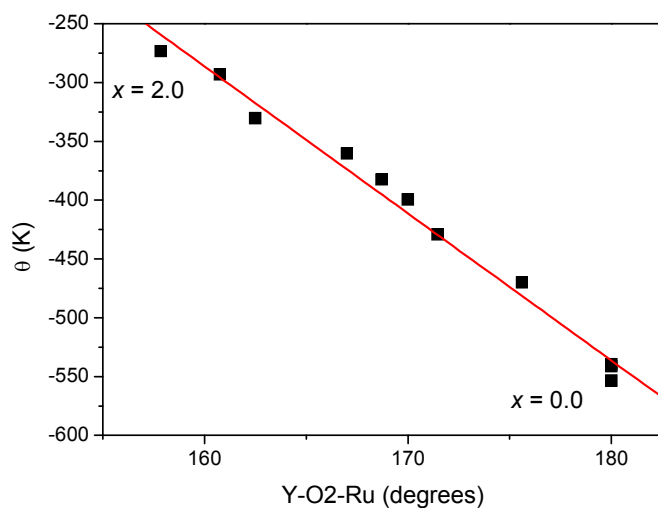


Figure 13. Relationship between the derived Weiss constant and the in-plane Y-O-Ru bond angle in the series $\text{Ba}_{2-x}\text{Sr}_x\text{YRuO}_6$. In the cubic structure there is a single O and all the Y-O-Ru angles are 180° . The line is a linear fit to the data.

Likewise at low Sr contents the maximum in the susceptibility, which is a proxy for T_N , decreases as the Sr content, and consequently distortion, increases but does not show a simple linear relationship. Although the observed linear relationship between the distortion and θ extends across the entire series this linear relationship does not extend to T_N at high Sr contents. Rather spin-reorientation leads to a dramatic change in the magnetic response. It appears that there is a delicate balance between the AF and FM in Sr_2YRuO_6 , that is disrupted by the addition of Ba which appears to diminish the strength of the FM coupling. Recall that Sr_2YRuO_6 has an I-type AFM structure in which the Ru moments form ferromagnetic (001) sheets that couple antiferromagnetically along [001], perpendicular to the YRuO plane. That long range AFM is observed requires either weak anisotropy in the crystal field or ferromagnetic exchange with the next nearest neighbours through long Ru-O-O-Ru superexchange chains.⁷ Cao *et al.*⁴⁶ found hysteresis in the magnetization of a single crystal sample of Sr_2YRuO_6 , consistent with a small ferromagnetic component. Although the structural studies show a small distortion of the RuO_6 octahedra, the most likely explanation for the dramatic changes in susceptibility at high Sr contents is that since the FM interactions are favoured by increasing distortions, at some critical angle there is a reversal of the net FM moment resulting in a transition between two AF spin structures. Reversal of the magnetisation, and even negative magnetization, has been observed in other perovskites containing a magnetic lanthanoid cation as a consequence of antiferromagnetic coupling

between this and the transition metal. This is clearly not the case here since Ru is the only magnetic cation. Mandal *et al.*⁴⁷ postulated that magnetization reversal in $\text{YFe}_{1-x}\text{Mn}_x\text{O}_3$ occurs as a result of disorder of the Fe and Mn resulting in a variety of magnetic exchange interactions. Granado *et al.*²⁰ provided evidence for a change in the long range spin order near 25 K in Sr_2YRuO_6 , that is near the minimum in susceptibility observed in their susceptibility measurements. They suggested that this was not a simple spin-reorientation rather that frustration effects induce two dimensional spin fluctuations around the maximum in susceptibility $T_N \sim 30$ K that transform to long range order around the susceptibility minimum. This behaviour was observed by Granado *et al.*²⁰ to be sensitive to the precise oxygen content of the sample perhaps suggesting that local disorder plays a role in relieving the magnetic frustration. As noted above our XANES measurements provide direct evidence for disorder in the current system. Further studies, and in particular neutron diffraction, are required to understand this unusual phenomena.

Conclusions

Synchrotron X-ray diffraction measurements have demonstrated that the series $\text{Ba}_{2-x}\text{Sr}_x\text{YRuO}_6$ displays the sequence of structures

$Fm\bar{3}m (a^0a^0a^0) \xrightarrow{x=0.6} I4/m (a^0a^0c^-) \xrightarrow{x=1.0} I2/m (a^-a^-c^0) \xrightarrow{x=1.4} P2_1/n (a^-a^-a^+)$ with the reduction in the average size of the A-site cation introducing tilting of the corner sharing octahedra. Variable temperature synchrotron measurements show that transitions between the structures can be induced by changing the temperature with high temperatures favouring higher symmetry structures. XANES spectroscopy confirms the oxidation states of the elements but reveals subtle changes in peak shapes consistent with changes in the local disorder. The unusual reversal in the magnetic susceptibility reported for Sr_2YRuO_6 has been confirmed and it is found that whilst this behaviour is impacted by the Sr:Ba content it does not correlate with the transition to the monoclinic structure. More detailed studies including neutron diffraction are required to establish the structural basis of this behaviour.

Acknowledgments

This work was, in part, performed at the Powder Diffraction and Soft X-ray beamlines at the Australian Synchrotron with the assistance of Drs Helen Brand, Bruce Cowie and Anton Tadich. BJK acknowledges the support of the Australian Research Council for this work.

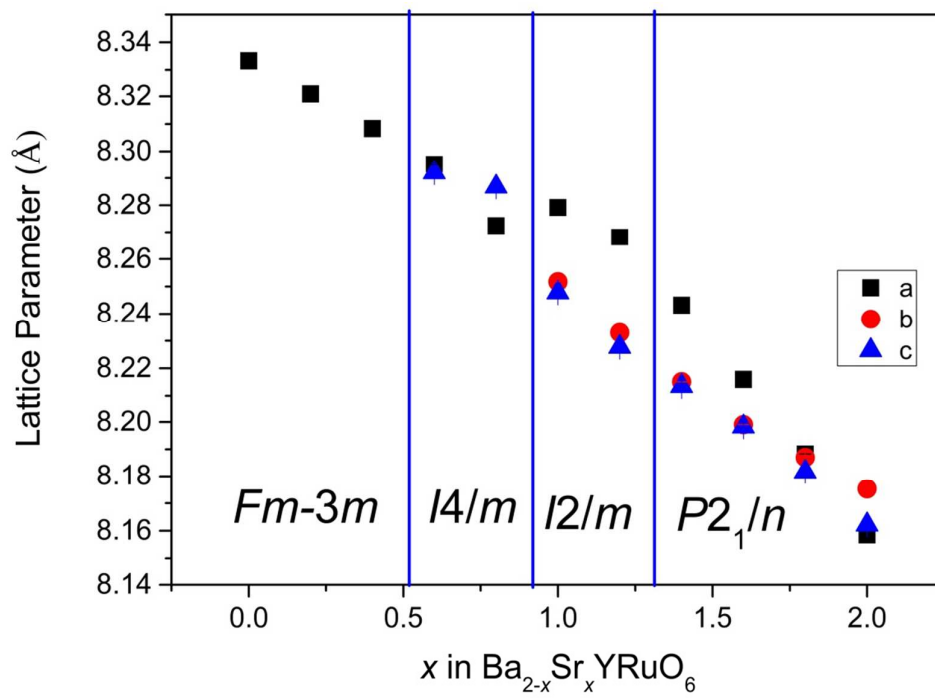
Table 1. Selected structural and magnetic properties for the series Ba_{2-x}Sr_xYRuO₆

<i>x</i>	0.0	0.2	0.4	0.6	0.8	1.0	1.2	1.4	1.6	1.8	2.0
Space Group	<i>Fm-3m</i>	<i>Fm-3m</i>	<i>Fm-3m</i>	<i>I4/m</i>	<i>I4/m</i>	<i>I2/m</i>	<i>I2/m</i>	<i>P2₁/n</i>	<i>P2₁/n</i>	<i>P2₁/n</i>	<i>P2₁/n</i>
<i>a</i> (Å)	8.333329(25)	8.32089(8)	8.30829(6)	5.86560(30)	5.8495(5)	5.85424(5)	5.84646(6)	5.82881(6)	5.80953(7)	5.78997(8)	5.76895(6)
<i>b</i> (Å)						5.83485(5)	5.82157(6)	5.80892(6)	5.79757(7)	5.78906(8)	5.78076(6)
<i>c</i> (Å)				8.29204(5)	8.28678(7)	8.24784(8)	8.22775(8)	8.21353(8)	8.19826(12)	8.18173(11)	8.16221(9)
β(°)						90.0935(1)	90.1548(1)	90.1832(2)	90.1978(2)	90.2208(2)	90.2468(2)
Vol (Å ³)	578.703(3)	576.115(9)	573.502(7)	285.290(3)	283.546(4)	281.734(4)	280.035(5)	278.101(5)	276.126(6)	274.237(6)	272.198(5)
<i>A</i> <i>x</i>						0.5003(18)	0.50106(18)	-0.00162(19)	-0.00271(20)	-0.00663(18)	-0.00681(18)
<i>y</i>						0	0	0.49018(9)	0.48439(6)	0.47869(6)	0.47334(6)
<i>z</i>						0.24955(15)	0.24925(15)	0.2510(1)	0.25081(14)	0.24909(14)	0.25119(12)
B _{iso} (Å ²)	0.97(1)	1.00(7)	1.05(7)	1.143(7)	1.113(10)	1.30(1)	1.54(1)	1.60(4)	1.66(4)	1.71(5)	1.729(8)
Y B _{iso} (Å ²)	1.35(2)	1.39(3)	1.30(2)	1.16(2)	1.16(2)	1.03(2)	1.11(3)	1.05(2)	0.95(2)	0.74(3)	0.86(2)
Ru B _{iso} (Å ²)	0.68(1)	0.67(2)	0.67(1)	0.76(2)	0.71(2)	0.75(2)	0.88(2)	0.91(2)	0.85(2)	1.01(3)	0.76(2)
O1 <i>x</i>	0.26563(33)	0.2668(4)	0.26833(31)	0	0	0.0363(8)	0.0478(7)	0.0555(7)	0.0560(7)	0.0624(7)	0.0624(6)
<i>y</i>				0	0	0	0	0.0016(8)	0.0069(5)	0.0103(5)	0.0134(4)
<i>z</i>				0.2837(10)	0.2734(8)	0.2674(7)	0.2677(6)	0.2645(6)	0.2669(6)	0.2727(5)	0.2688(5)
B _{iso} (Å ²)	1.50(4)	1.38(5)	1.38(4)	3.46(23)	1.97(18)	1.49(15)	1.47(14)	1.34(14)	0.80(4)	1.47(5)	1.02(10)
O2 <i>x</i>				0.2523(9)	0.2469(7)	0.2730(5)	0.2720(5)	0.2608(14)	0.2552(10)	0.2447(9)	0.2419(7)
<i>y</i>				0.2716(15)	0.2841(8)	0.2665(7)	0.2679(7)	0.2920(12)	0.3006(10)	0.2973(9)	0.3006(7)
<i>z</i>				0	0	-0.0216(4)	-0.0246(4)	-0.0232(10)	-0.0306(8)	-0.0332(7)	-0.0388(6)
B _{iso} (Å ²)				0.62(9)	1.62(10)	1.60(12)	2.01(3)	3.66(21)	1.77(9)	1.29(5)	0.85(10)
O3 <i>x</i>								0.2662(11)	0.2888(10)	0.3003(9)	0.3067(7)
<i>y</i>								0.7526(10)	0.7530(9)	0.7599(9)	0.7603(7)
<i>z</i>								-0.0322(7)	-0.0332(9)	-0.0308(7)	-0.0354(5)
B _{iso} (Å ²)								0.35(14)	1.52(8)	1.33(5)	1.09(10)
Ru-O1 (Å)	1.9531(28)	1.9406(32)	1.9248(26)	1.794(8)	1.878(7)	1.9361(6)	1.933(5)	1.943(5)	1.940(4)	1.898(4)	1.924(4)
Ru-O2 (Å)				1.976(5)	1.946(4)	1.9114(3)	1.908(3)	1.858(6)	1.849(7)	1.901(6)	1.908(4)
Ru-O3 (Å)								1.986(5)	1.931(6)	1.917(6)	1.894(4)
Y-O1 (Å)	2.2136(28)	2.2198(32)	2.2293(26)	2.352(8)	2.266(7)	2.215(6)	2.219(5)	2.214(5)	2.211(5)	2.259(4)	2.223(4)
Y-O2 (Å)				2.175(5)	2.202(4)	2.237(3)	2.237(3)	2.283(6)	2.303(6)	2.251(5)	2.252(4)
Y-O3 (Å)								2.167(5)	2.223(5)	2.238(5)	2.267(4)
B-O _{avg} (Å)	2.083	2.080	2.077	2.075	2.073	2.075	2.074	2.075	2.076	2.077	2.078
Y-O1-Ru (°)	180	180	180	180	180	168.18(25)	164.45(22)	162.00(23)	161.75(23)	159.54(22)	159.44(19)
Y-O2-Ru (°)				175.6(4)	171.46(26)	169.99(17)	168.70(18)	167.0(5)	162.49(31)	160.75(25)	157.85(20)

Y-O3-Ru (°)								164.4(4)	162.08(33)	160.28(25)	157.72(21)
B-O-B _{avg} (°)	180	180	180	177.80	175.73	169.09	166.58	164.5	162.11	160.19	158.33
Θ/K	-539.67	-553.60	-541.53	-470.25	-429.26	-399.50	-382.42	-360.49	-330.35	-293.14	-273.54
μ _{obs} (BM)	4.11	4.15	4.17	3.99	3.90	3.85	3.88	3.88	3.85	3.79	3.73
Y BVS	3.55	3.49	3.40	3.44	3.47	3.40	3.38	3.50	3.27	3.22	3.24
Ru BVS	5.20	5.38	5.61	5.92	5.65	5.72	5.74	5.60	5.93	5.91	5.86

1. S. M. Kazakov, C. Chaillout, P. Bordet, J. J. Capponi, M. NunezRegueiro, A. Rysak, J. L. Tholence, P. G. Radaelli, S. N. Putilin and E. V. Antipov, *Nature*, 1997, **390**, 148-150.
2. K. L. Kobayashi, T. Kimura, H. Sawada, K. Terakura and Y. Tokura, *Nature*, 1998, **395**, 677-680.
3. Y. Tomioka, T. Okuda, Y. Okimoto, R. Kumai, K. I. Kobayashi and Y. Tokura, *Physical Review B*, 2000, **61**, 422-427.
4. H. L. Feng, M. Arai, Y. Matsushita, Y. Tsujimoto, Y. F. Guo, C. I. Sathish, X. Wang, Y. H. Yuan, M. Tanaka and K. Yamaura, *Journal of the American Chemical Society*, 2014, **136**, 3326-3329.
5. J. P. Carlo, J. P. Clancy, K. Fritsch, C. A. Marjerrison, G. E. Granroth, J. E. Greedan, H. A. Dabkowska and B. D. Gaulin, *Physical Review B*, 2013, **88**.
6. T. Aharen, J. E. Greedan, C. A. Bridges, A. A. Aczel, J. Rodriguez, G. MacDougall, G. M. Luke, V. K. Michaelis, S. Kroeker, C. R. Wiebe, H. D. Zhou and L. M. D. Cranswick, *Physical Review B*, 2010, **81**.
7. J. E. Greedan, *Journal of Materials Chemistry*, 2001, **11**, 37-53.
8. G. Long, M. DeMarco, D. Coffey, M. K. Toth and M. S. Torikachvili, *Physical Review B*, 2013, **87**.
9. S. Garcia and L. Ghivelder, *Solid State Communications*, 2014, **179**, 11-15.
10. P. D. Battle and C. W. Jones, *Journal of Solid State Chemistry*, 1989, **78**, 108-116.
11. P. D. Battle and W. J. Macklin, *Journal of Solid State Chemistry*, 1984, **52**, 138-145.
12. M. T. Anderson, K. B. Greenwood, G. A. Taylor and K. R. Poeppelmeier, *Prog. Solid State Chem.*, 1993, **22**, 197-233.
13. C. J. Howard, B. J. Kennedy and P. M. Woodward, *Acta Crystallographica Section B-Structural Science*, 2003, **59**, 463-471.
14. B. J. Kennedy, B. A. Hunter and J. R. Hester, *Physical Review B*, 2002, **65**.
15. R. P. Singh and C. V. Tomy, *Journal of Physics-Condensed Matter*, 2008, **20**.
16. R. P. Singh and C. V. Tomy, *Physical Review B*, 2008, **78**, 024432.
17. S. M. Rao, J. K. Srivastava, M. K. Wu, B. H. Mok, C. L. Chen, M. C. Ling, H. L. Liu, Y. Y. Chen and J. C. Ho, *Journal of Superconductivity and Novel Magnetism*, 2011, **24**, 1249-1262.
18. M. K. Wu, D. Y. Chen, F. Z. Chien, S. R. Sheen, D. C. Ling, C. Y. Tai, G. Y. Tseng, D. H. Chen and F. C. Zhang, *Zeitschrift Fur Physik B-Condensed Matter*, 1997, **102**, 37-41.
19. P. L. Bernardo, L. Ghivelder, G. G. Eslava, H. S. Amorim, E. H. C. Sinnecker, I. Felner, J. J. Neumeier and S. Garcia, *Journal of Physics-Condensed Matter*, 2012, **24**.
20. E. Granado, J. W. Lynn, R. F. Jardim and M. S. Torikachvili, *Physical Review Letters*, 2013, **110**.
21. T. Aharen, J. E. Greedan, F. Ning, T. Imai, V. Michaelis, S. Kroeker, H. D. Zhou, C. R. Wiebe and L. M. D. Cranswick, *Physical Review B*, 2009, **80**.
22. K. S. Wallwork, B. J. Kennedy and D. Wang, *AIP Conference Proceedings*, 2007, **879**, 879-882.
23. A. C. Larson and R. B. Von Dreele, *General Structure Analysis System. LANSCE, MS-H805, Los Alamos, New Mexico*, 1994.
24. B. C. C. Cowie, A. Tadich and L. Thomsen, *AIP Conference Proceedings*, 2010, **1234**, 307-310.
25. P. E. R. Blanchard, Z. X. Huang, B. J. Kennedy, S. Liu, W. Miiller, E. Reynolds, Q. Zhou, M. Avdeev, Z. Zhang, J. B. Aitken, B. C. C. Cowie, L. Y. Jang, T. T. Tan, S. Li and C. D. Ling, *Inorganic Chemistry*, 2014, **53**, 952-960.
26. P. E. R. Blanchard, S. Liu, B. J. Kennedy, C. D. Ling, Z. Zhang, M. Avdeev, B. C. C. Cowie, L. Thomsen and L.-Y. Jang, *Dalton Trans.*, 2013, **42**, 14875-14882.
27. B. Ravel and M. Newville, *J. Synchrotron Rad.*, 2005, **12**, 537-541.
28. Q. D. Zhou, B. J. Kennedy, C. J. Howard, M. M. Elcombe and A. J. Studer, *Chemistry of Materials*, 2005, **17**, 5357-5365.
29. Q. D. Zhou, B. J. Kennedy and M. M. Elcombe, *Journal of Solid State Chemistry*, 2007, **180**, 541-548.
30. Q. D. Zhou, T. Y. Tan, B. J. Kennedy and J. R. Hester, *Journal of Solid State Chemistry*, 2013, **206**, 122-128.

31. N. Narayanan, D. Mikhailova, A. Senyshyn, D. M. Trots, R. Laskowski, P. Blaha, K. Schwarz, H. Fuess and H. Ehrenberg, *Physical Review B*, 2010, **82**, 024403.
32. Q. D. Zhou and B. J. Kennedy, *Journal of Solid State Chemistry*, 2005, **178**, 3589-3594.
33. W. Miiller, M. Avdeev, Q. D. Zhou, A. J. Studer, B. J. Kennedy, G. J. Kearley and C. D. Ling, *Physical Review B*, 2011, **84**.
34. B. J. Kennedy, C. J. Howard and B. C. Chakoumakos, *Journal of Physics-Condensed Matter*, 1999, **11**, 1479-1488.
35. Z. M. Zhang, S. C. Middleburgh, M. de los Reyes, G. R. Lumpkin, B. J. Kennedy, P. E. R. Blanchard, E. Reynolds and L. Y. Jang, *J. Phys. Chem. C*, 2013, **117**, 26740-26749.
36. Q. D. Zhou, B. J. Kennedy, Z. M. Zhang, L. Y. Jang and J. B. Aitken, *Chem. Mater.*, 2009, **21**, 4203-4209.
37. Z. Hu, H. von Lips, M. S. Golden, J. Fink, G. Kaindl, F. M. F. de Groot, S. Ebbinghaus and A. Reller, *Phys. Rev. B*, 2000, **61**, 5262-5266.
38. N. Thromat, C. Noguera, M. Gautier, F. Jollet and J. P. Duraud, *Phys. Rev. B*, 1991, **44**, 7904-7911.
39. M. A. Carpenter, E. K. H. Salje and A. Graeme-Barber, *European Journal of Mineralogy*, 1998, **10**, 621-691.
40. Z. M. Zhang, B. J. Kennedy, C. J. Howard, M. A. Carpenter, W. Miiller, K. S. Knight, M. Matsuda and M. Miyake, *Physical Review B*, 2012, **85**, 174110.
41. C. Sakai, Y. Doi, Y. Hinatsu and K. Ohoyama, *Journal of Physics-Condensed Matter*, 2005, **17**, 7383-7394.
42. A. Sasaki, Y. Doi and Y. Hinatsu, *Journal of Alloys and Compounds*, 2009, **477**, 900-904.
43. P. G. Radaelli, G. Iannone, M. Marezio, H. Y. Hwang, S. W. Cheong, J. D. Jorgensen and D. N. Argyriou, *Physical Review B*, 1997, **56**, 8265-8276.
44. C. Ritter, M. R. Ibarra, L. Morellon, J. Blasco, J. Garcia and J. M. De Teresa, *Journal of Physics-Condensed Matter*, 2000, **12**, 8295-8308.
45. A. K. Prodjosantoso, Q. D. Zhou and B. J. Kennedy, *Journal of Solid State Chemistry*, 2013, **200**, 241-245.
46. G. Cao, Y. Xin, C. S. Alexander and J. E. Crow, *Physical Review B*, 2001, **63**, 184432.
47. P. Mandal, C. R. Serrao, E. Suard, V. Caignaert, B. Raveau, A. Sundaresan and C. N. R. Rao, *Journal of Solid State Chemistry*, 2013, **197**, 408-413.



Doping Ba_2YRuO_6 with Sr induces octahedral tilting and significantly impacts on the magnetic properties